

Quantum Dissipative Continuous Time Crystals

Felix Russo[✉]* and Thomas Pohl[†]

Institute for Theoretical Physics, Vienna University of Technology (TU Wien), Vienna, Austria

(Dated: March 21, 2025)

Continuous time crystals, i.e., nonequilibrium phases with a spontaneously broken continuous time-translational symmetry, have been studied and recently observed in the long-time dynamics of open quantum systems. Here, we investigate a lattice of interacting three-level systems and find two distinct time-crystal phases that cannot be described within mean-field theory. Remarkably, one of them emerges only in the presence of quantum fluctuations. Our findings extend explorations of continuous time-translational symmetry breaking in dissipative systems beyond the classical phenomenology of periodic orbits in a low-dimensional nonlinear system. The proposed model applies directly to the laser-driven dynamics of interacting Rydberg states in neutral atom arrays and suggests that the predicted time-crystal phases are observable in such experiments.

The concept of symmetry breaking is instrumental in understanding a broad range of fundamental processes in physics, chemistry, and biology [1]. Among the most ubiquitous examples is the emergence of ordered structures from an otherwise homogeneous system. In recent years, the question of whether translational symmetry could be broken in the fourth dimension has attracted much attention [2–4]. A quantum system that self-organizes in time, i.e., a time crystal, represents a new exotic state of matter. Early theoretical work focused on discrete time-translational symmetry breaking in periodically driven systems [5–7], which has subsequently been observed in different experimental platforms [8–16]. The possibility of continuous time-translational symmetry breaking was pointed out in [17] in the form of a so-called boundary time crystal, where a fraction of a many-body system can undergo spontaneous oscillations. The emergence of a continuous time crystal (CTC) phase in this setting is directly connected to the physics of dissipative quantum systems, which can exhibit limit-cycle solutions [17–20] that were recently observed experimentally in nonlinear optical cavities [21, 22], optical metamaterials [23], thermal Rydberg vapors [24], and semiconductors [25].

Despite the diversity of physical platforms and models, an overarching question has been whether time-translational symmetry breaking can be understood as an inherently classical phenomenon and to what extent quantum mechanics determines the properties of time crystal phases [17, 20, 26–29]. In current experiments and theoretical models, the emergence of CTC phases in dissipative quantum many-body systems is largely understood in terms of a classical mean-field picture. Hereby, the dynamics of single-particle observables are governed by a small set of nonlinear equations of motion that can exhibit limit-cycle attractors. In fact, the emergence of persistent oscillations in open quantum systems can be associated with an approach to the classical limit [30],

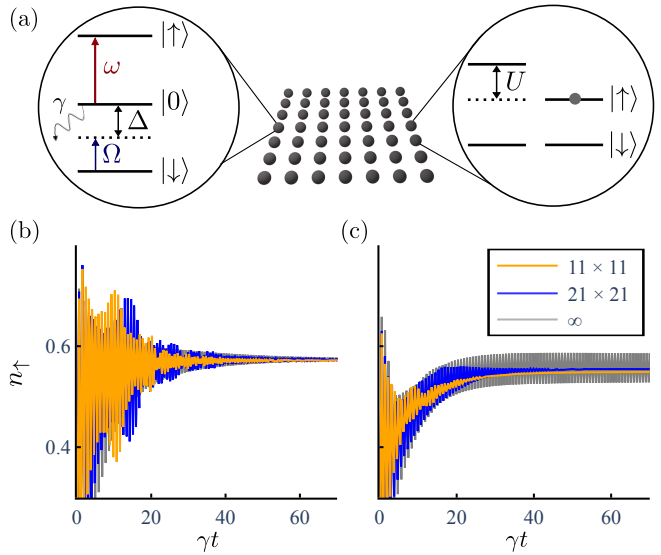


FIG. 1. (a) The three levels of spin-1 particles in a two-dimensional lattice are subject to an energy mismatch Δ and coupled by two external fields with Rabi frequencies Ω and ω . The interplay of this coupling with dissipative decay at a rate γ and mutual dipole-dipole interactions $U \sim 1/r^3$ can lead to persistent oscillations of the level populations. While mean-field theory predicts a stationary steady state for the chosen set of parameters (b), persistent oscillations are found to emerge in the thermodynamical limit upon accounting for quantum fluctuations (c). Such a quantum dissipative time crystal phase, thus, breaks the continuous time translational symmetry of the system in the absence of a limit cycle in the classical mean-field dynamics.

while quantum-mechanical extensions of mean-field models have so far been found to cause damping of semiclassical limit cycles [26, 31]. Hence, there is currently no experimental or theoretical evidence for continuous quantum time crystal (qCTC) phases in open quantum systems that do not pertain to the limit-cycle phenomenology of nonlinear mean-field equations.

Here, we address this question by exploring the dissipative dynamics of a spin-1 lattice with finite-range interactions that do not afford an exact mean-field de-

* felix.russo@tuwien.ac.at

† thomas.pohl@itp.tuwien.ac.at

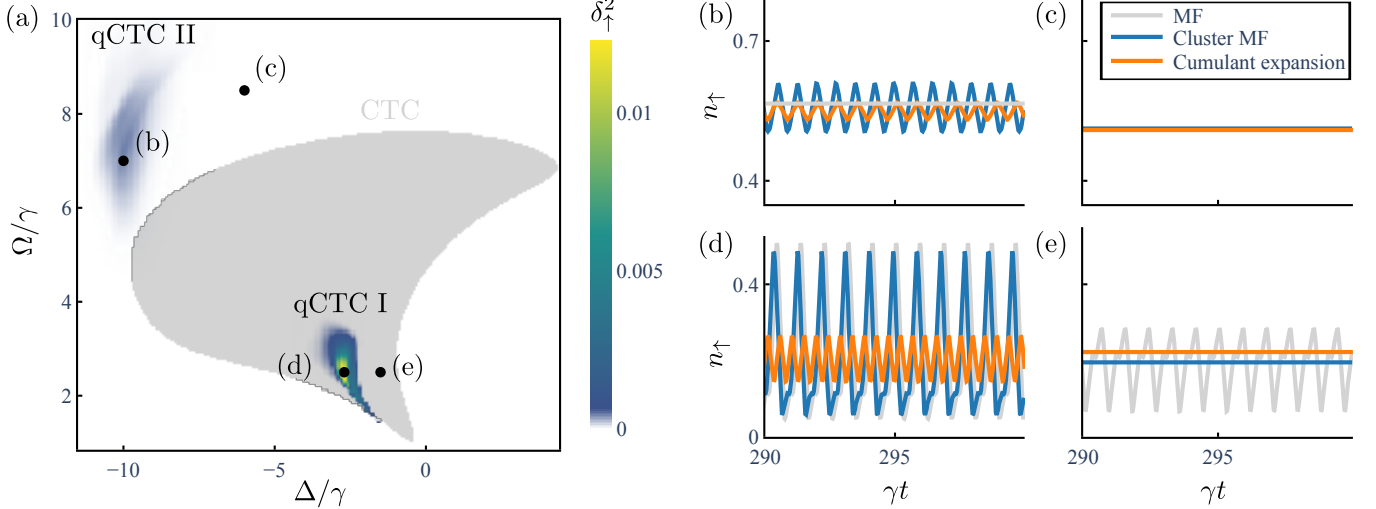


FIG. 2. (a) Phase diagram in the thermodynamic limit for $\omega = 6\gamma$ and $\chi = -18\gamma$. The occurrence of mean-field CTCs is marked by the gray shaded area. The superimposed color map shows the asymptotic oscillations contrast δ_1^2 (see Eq.(7)) from beyond mean-field calculations, revealing two distinct oscillatory regions, which we term type-I and type-II qCTC. The qCTC-I phase resides within the mean-field CTC region, while the classical mean-field CTC is otherwise damped by quantum fluctuations, as illustrated in panels (d) and (e), respectively. In contrast, time-translational symmetry breaking in the qCTC-II phase occurs outside the classical CTC region and is driven by quantum fluctuations, as shown in panels (b) and (c). The oscillation contrast in panel (a) is obtained from a 2nd-order cumulant expansion, while panels (b)-(e) compare mean-field dynamics to the results of the cumulant expansion and cluster mean-field simulations described in the text.

scription. Numerical simulations reveal two distinct time crystalline phases with persistent oscillations of one-body observables in the thermodynamic limit. The first kind is found under conditions for which limit cycle dynamics are predicted by mean-field theory but survive in the presence of significant quantum fluctuations. In addition, we identify a second type of qCTC that is not predicted by mean-field theory but instead is driven by quantum fluctuations. This phase features a distinct scaling of quantum fluctuations with system size and emerges in the absence of long-range correlations, consistent with the phenomenology of oscillatory solutions in quenched isolated quantum systems [32]. The found qCTC phases do not rely on symmetries of the underlying master equation and are robust to perturbations, both of which are essential aspects for potential experiments. Indeed, the studied model and considered parameters for qCTC should be realizable in current quantum simulation experiments with optical tweezer arrays of Rydberg atoms.

We consider a two-dimensional cubic lattice of three-level systems with quantum states $|\downarrow\rangle$, $|\uparrow\rangle$, and $|0\rangle$, as illustrated in Figure 1(a). The intermediate state $|0\rangle$ is coupled to the upper $|\uparrow\rangle$ and lower $|\downarrow\rangle$ states with respective coupling strengths ω and Ω , and there is an energy difference Δ between the ground state $|\downarrow\rangle$ and the excited states. The corresponding Hamiltonian for N such

three-level systems can be written as

$$\hat{H} = \Delta \sum_i \hat{n}_\downarrow^{(i)} + \sum_i \left(\Omega \hat{\sigma}_{\downarrow 0}^{(i)} + \omega \hat{\sigma}_{\uparrow 0}^{(i)} + \text{h.c.} \right) + \sum_{i < j} U_{ij} \hat{n}_\uparrow^{(i)} \hat{n}_\uparrow^{(j)}, \quad (1)$$

where $\hat{\sigma}_{\alpha\beta}^{(i)} = |\alpha\rangle_i \langle \beta|$ denote the transition operators for the i^{th} particle, and $\hat{n}_\alpha^{(i)} = \hat{\sigma}_{\alpha\alpha}^{(i)}$ corresponds to the respective excitation density at a given site. The second line in Eq.(1) describes interactions between particles in the uppermost state $|\uparrow\rangle$. We consider power-law potentials $U_{ij} = C_\alpha / r_{ij}^\alpha$, where C_α is the interaction strength and $r_{ij} = |\mathbf{r}_j - \mathbf{r}_i|$ the distance between two particles i and j at positions \mathbf{r}_i and \mathbf{r}_j in the lattice. We parameterize the interaction strength by the total interaction energy $\chi = \sum_{j \neq 0} U_{0j}$ of the particle at position \mathbf{r}_0 in the center of the lattice with all surrounding spins.

This Hamiltonian applies directly to current experiments with neutral-atom tweezer arrays [33–37], where $|\downarrow\rangle$ corresponds to an atomic ground state, $|0\rangle$ to a low-lying intermediate state, and $|\uparrow\rangle$ to a highly excited Rydberg state. Laser fields can be used to drive the $|0\rangle \leftrightarrow |\downarrow\rangle$ and $|0\rangle \leftrightarrow |\uparrow\rangle$ transitions with Rabi frequencies Ω and ω , as described by Eq.(1). Considering resonant laser driving of the upper transition, the frequency detuning on the lower transition corresponds to the energy mismatch Δ in Eq.(1). Moreover, Rydberg atoms feature strong van der Waals interactions, $U_{ij} = C_6 / r_{ij}^6$, [38–40] while longer ranged dipole-dipole interactions, $U_{ij} = C_3 / r_{ij}^3$,

can be realized and controlled via microwave dressing of the Rydberg state [41–43]. While Rydberg states ($|\uparrow\rangle$) typically feature very long lifetimes [38, 39, 44, 45], the radiative decay of the intermediate $|0\rangle$ -state introduces dissipation as described by the Lindbladian

$$\hat{\mathcal{L}}(\hat{\rho}) = \sum_i \gamma \hat{\sigma}_{0\downarrow}^{(i)} \hat{\rho} \hat{\sigma}_{0\downarrow}^{(i)} - \frac{\gamma}{2} \{ \hat{n}_0^{(i)}, \hat{\rho} \} \quad (2)$$

with a spontaneous decay rate γ . The dynamics of the N -body density matrix $\hat{\rho}$ of the lattice is determined by the quantum master equation

$$\frac{\partial}{\partial t} \hat{\rho} = i[\hat{\rho}, \hat{H}] + \hat{\mathcal{L}}(\hat{\rho}). \quad (3)$$

Its exact solution can, however, be found numerically only for small particle numbers, such that suitable approximations are required to analyze the nonequilibrium physics of large lattices.

The simplest approach is to entirely neglect correlations by factorizing two-body observables

$$\langle \hat{\sigma}_{\alpha\beta}^{(i)} \hat{\sigma}_{\bar{\alpha}\bar{\beta}}^{(j)} \rangle \approx \sigma_{\alpha\beta}^{(i)} \sigma_{\bar{\alpha}\bar{\beta}}^{(j)} \quad (4)$$

to obtain a set of coupled mean-field equations for the one-body expectation values $\sigma_{\alpha\beta}^{(i)} = \langle \hat{\sigma}_{\alpha\beta}^{(i)} \rangle$ that can be readily solved and have been used to study steady-state phases in different open quantum systems [18, 21, 22, 24, 31, 46–49]. In many cases, the nonlinearity that arises from the mean-field interaction can give rise to bistabilities [46, 50–52] that can often be related to a first-order nonequilibrium phase transition of the exact quantum dynamics [53]. As pointed out in [24], interacting multi-level systems can also support the formation of nonstationary phases, where the system settles into a state with persistent periodic oscillations in the long-time limit. Figure 2a shows the parameter region where we find such a CTC phase with broken time translational symmetry from a linear stability analysis of the mean-field equations obtained from Eq.(3). Indeed, the basic idea of CTC phases in an open quantum many-body system [17] is often based on the validity of mean-field theory. In the present case, this would require $\alpha \leq 2$ such that interactions are long-ranged in two dimensions and the mean-field contribution to the interaction dominates in the thermodynamic limit.

Consequently, classical mean-field theory does not straightforwardly apply to the physics of neutral-atom arrays, where relevant interactions, such as van der Waals ($\alpha = 6$) and dipole-dipole ($\alpha = 3$) interactions, are shorter-ranged. Various methods have recently been explored [54] to study the dissipative dynamics of quantum many-body systems beyond simplified mean-field models. Here, we employ two complementary approaches to account for quantum correlations and fluctuations in lattices with dipole-dipole interactions ($\alpha = 3$).

First, we use a cumulant expansion that permits a systematic inclusion of correlations through a hierarchy of

equations for multi-particle cumulants of increasing order [55–60]. We take 2nd-order correlations into account

$$\langle \hat{\sigma}_{\alpha\beta}^{(i)} \hat{\sigma}_{\bar{\alpha}\bar{\beta}}^{(j)} \rangle = \sigma_{\alpha\beta}^{(i)} \sigma_{\bar{\alpha}\bar{\beta}}^{(j)} + \langle \hat{\sigma}_{\alpha\beta}^{(i)} \hat{\sigma}_{\bar{\alpha}\bar{\beta}}^{(j)} \rangle_c. \quad (5)$$

but neglect three-particle cumulants to truncate the hierarchy of equations [61]. Second, we perform cluster mean-field simulations [62], whereby the density matrix is factorized

$$\hat{\rho} = \bigotimes_i \hat{\rho}_{\mathcal{C}_i} \quad (6)$$

into finite clusters, \mathcal{C}_i , of particles. Using this ansatz in the master equation (3), one obtains the exact quantum dynamics on each plaquette \mathcal{C}_i , while interactions between particles in different clusters are included on a mean-field level. In the thermodynamic limit, one can assume homogeneity such that all plaquettes become identical, $\hat{\rho}_{\mathcal{C}_i} = \hat{\rho}_{\mathcal{C}}$ [61].

While either method is approximate, they provide complementary approaches to include quantum fluctuations. In the cumulant expansion, we account only for direct binary correlations but do so for all particle distances throughout the lattice. On the other hand, the cluster mean-field simulations treat correlations only within a finite interaction range but include all orders of correlations via an exact solution of the master equation within a chosen plaquette \mathcal{C} . Through this complementarity, the application and comparison of both methods affords more stringent conclusions about the emergence of quantum time-crystalline phases.

In order to detect oscillatory solutions in such simulations we use the time-averaged standard deviation

$$\delta_{\uparrow}^2 = \frac{1}{\tau} \int_t^{t+\tau} n_{\uparrow}(t')^2 dt' - \left(\frac{1}{\tau} \int_t^{t+\tau} n_{\uparrow}(t') dt' \right)^2 \quad (7)$$

of the Rydberg-state density, $n_{\uparrow} = N^{-1} \sum_i \langle \hat{n}_{\uparrow}^{(i)} \rangle$, in the long-time limit ($t \rightarrow \infty$) and increase τ until δ_{\uparrow}^2 is converged. By construction, δ_{\uparrow}^2 vanishes for stationary steady states and yields a measure of the oscillation amplitude of n_{\uparrow} in the time-crystal phase.

Figure 2(a) shows how the phase diagram is modified upon including quantum correlations via the 2nd-order cumulant expansion. For most parameters, the boundary time-crystal phase predicted by mean-field theory is expectedly damped upon inclusion of quantum fluctuations, as illustrated in Figure 2(e). Remarkably, however, we find a small but finite parameter region where the time-crystalline phase persists in the presence of correlations. We denote this form of quantum time crystals as qCTC-I and have confirmed their existence both via the cumulant expansion and cluster mean-field simulations, as shown in Figure 2(d). Surprisingly, we find another time-crystal phase, marked as qCTC-II in Figure 2(a). This type-II oscillatory solution emerges outside the classical mean-field regime, i.e., in a parameter region where the

mean-field solution settles into a stationary steady state. Rather than damping the mean-field dynamics, accounting for correlations causes a breaking of time-translation symmetry. Oscillations in this novel time-crystal phase are thus driven by quantum fluctuations, as shown in Figure 2(b).

For a more detailed analysis of the two qCTC phases, we study the variance

$$\Delta N_{\uparrow}^2 = \langle \hat{N}_{\uparrow}^2 \rangle - \langle \hat{N}_{\uparrow} \rangle^2, \quad (8)$$

of the total population in the $|\uparrow\rangle$ -state, given by $\hat{N}_{\uparrow} = \sum_i \hat{n}_{\uparrow}^{(i)}$. For boundary time crystals with all-to-all interactions [17], pertinent to mean-field theory, it was found that fluctuations of the type $F^2 = \Delta N_{\uparrow}^2/N$ [63–69] grow linearly with the number N of particles while remaining finite for stationary steady states [48]. As shown in Figures 3(a) and (c), this behavior is recovered in the qCTC-I phase of our system. In stark contrast, however, in the qCTC-II phase, we find a sublinear growth of F^2 upon increasing the particle number N . While the observed increase of F^2 still distinguishes the time crystal from the stationary phase, the observed weak power-law dependence $F^2 \sim N^{0.06}$ differs distinctively from the linear mean-field scaling of the qCTC-I time crystal [61]. Notably, this implies that the relative uncertainty $\Delta N_{\uparrow}/N_{\uparrow}$ approaches a finite value as $N \rightarrow \infty$ for the type-I time crystal while it vanishes in the thermodynamic limit of the qCTC-II phase. This behavior is consistent with the results of [32], where it was shown that persistent oscil-

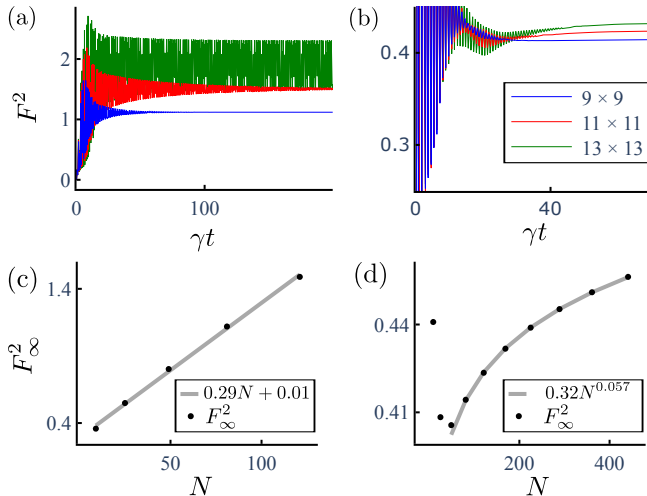


FIG. 3. Dynamics of the normalized variance $F^2 = \Delta N_{\uparrow}^2/N$ in the (a) qCTC-I and the (b) qCTC-II phase. Panels (c) and (d) show the corresponding dependence of steady-state value $F_{\infty}^2 = \lim_{t \rightarrow \infty} F^2$ on the particle number N . The interaction strength was fixed to $\chi = -18\gamma$ for all system sizes. Since the longer-lived oscillations in qCTC-I prevent reaching a steady state within reasonable simulation times for large systems, we show less data points in (c).

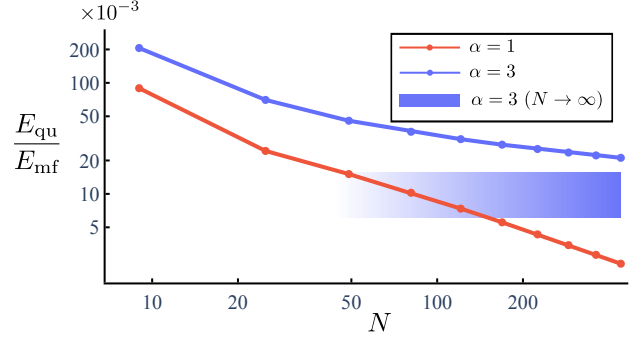


FIG. 4. Ratio between correlation and mean-field energy for a long ($\alpha = 1$) and a short-range ($\alpha = 3$) interaction potential. Parameters are taken from qCTC-II. In the long-range case, the energy ratio tends to 0 as the thermodynamic limit is approached. In the short-range case, on the other hand, the correlations remain non-negligible as $N \rightarrow \infty$, and the energy ratio fluctuates between finite values due to the broken time-translation symmetry. The oscillation range in the thermodynamic limit for $\alpha = 3$ is depicted as a light blue area. For all system sizes and potentials, the interaction strength was fixed to $\chi = -18\gamma$.

lations can emerge in quenched isolated quantum many-body systems in the absence of long-range spatial correlations, demonstrating that spatial long-range order is irrelevant for time-translational symmetry breaking.

Despite the sublinear scaling behavior in qCTC-II, quantum fluctuations have a significant effect on the dynamics of the system in either phase, owing to the finite-range nature of the interaction. We can quantify the impact of correlations by comparing the total mean-field interaction energy

$$E_{\text{mf}} = \sum_{i,j>i} U_{ij} n_{\uparrow}^{(i)} n_{\uparrow}^{(j)} \quad (9)$$

to the correlation energy

$$E_{\text{qu}} = \sum_{i,j>i} U_{ij} \langle \hat{n}_{\uparrow}^{(i)} \hat{n}_{\uparrow}^{(j)} \rangle_c. \quad (10)$$

As shown in Figure 4 for the qCTC-II phase, the ratio $E_{\text{qu}}/E_{\text{mf}}$ indeed approaches a finite value in the thermodynamic limit [61]. In contrast, an exact description via mean-field theory requires $E_{\text{qu}}/E_{\text{mf}}$ to vanish in the thermodynamic limit, which is the case for long-range interacting systems [21, 22, 26, 31, 48, 49]. This is illustrated numerically in Figure 4 for a long-range interacting lattice with $\alpha = 1$ and otherwise identical parameters. Thus, we conclude that the qCTC-II time-crystal phase can be considered a quantum effect beyond the classical dynamics of boundary time crystals in the mean-field regime.

In summary, we have studied the dissipative dynamics of interacting three-level quantum systems and found nonequilibrium phases with persistent oscillations that extend the classical mean-field phenomenology of CTC

phases. In particular, we have shown that continuous time-translational symmetry can be broken as a direct consequence of quantum correlations. Fluctuations in such quantum continuous time crystals (here termed qCTC-II) exhibit distinctly different scaling behavior than found in mean-field models with long-range interactions [48].

The reported dynamics of spin-1 lattices could not be found in equivalent spin-1/2 systems, raising interesting questions regarding the fundamental requirements for the emergence of CTC phases and motivating further explorations of minimal models for qCTCs in many-body systems. Addressing these issues could expand the understanding of the basic mechanisms for CTC formation in open quantum systems, possibly beyond the phenomenology of periodic orbits in classical nonlinear systems, and may yield a suitable classification of distinct time-crystalline phases.

Our model applies directly to the physics of neutral atom arrays[33–37], which should make detailed experimental explorations of the predicted time crystalline dynamics possible. Here, the qCTC-II phase appears particularly attractive as the intermediate-state population turns out to be very small in the oscillating phase. The type-II time crystal, thus, forms an approximate dark state in which persistent oscillations primarily occur between the $|\downarrow\rangle$ - and $|\uparrow\rangle$ -state, such that heating

of the atoms due to photon emission from the $|0\rangle$ -state remains at a low level [61]. The parameters considered in this work are typical for tweezer arrays of rubidium atoms. The considered Rabi frequencies of around $\sim 10\gamma$ correspond to readily achievable values of $\sim 13\text{MHz}$ for two-photon excitation of nS -Rydberg states via the intermediate $6P$ -state [70]. The chosen interaction strength of $\chi = -18\gamma$ would correspond to a modest nearest-neighbor interaction of $C_3/a^3 = -2.6\text{MHz}$, which can be realized experimentally by off-resonant microwave dressing [42] of a $|nS\rangle$ -Rydberg state with a $|nP\rangle$ -state, enabling a strong resonant dipole-dipole interaction.

We thank Fan Yang, Jan Kumlin, Andreas Nunnenkamp, and Simon P. Pedersen for insightful discussions. This work was supported by funding from the Austrian Science Fund (Grant No. 10.55776/COE1) and the European Union (NextGenerationEU), by the SNSF through the Swiss Quantum Initiative, and from the European Research Council through the ERC Synergy Grant SuperWave (Grant No. 101071882).

Note added: During preparation of this manuscript, we became aware of a related work on time-crystal phases in open spin chains with power-law interactions [71].

[1] F. Strocchi, *Symmetry breaking*, Vol. 643 (Springer, 2005).

[2] F. Wilczek, Quantum time crystals, *Physical review letters* **109**, 160401 (2012).

[3] K. Sacha and J. Zakrzewski, Time crystals: a review, *Reports on Progress in Physics* **81**, 016401 (2017).

[4] M. P. Zaletel, M. Lukin, C. Monroe, C. Nayak, F. Wilczek, and N. Y. Yao, Colloquium: Quantum and classical discrete time crystals, *Reviews of Modern Physics* **95**, 031001 (2023).

[5] K. Sacha, Modeling spontaneous breaking of time-translation symmetry, *Physical Review A* **91**, 033617 (2015).

[6] D. V. Else, B. Bauer, and C. Nayak, Floquet time crystals, *Physical review letters* **117**, 090402 (2016).

[7] V. Khemani, A. Lazarides, R. Moessner, and S. L. Sondhi, Phase structure of driven quantum systems, *Physical review letters* **116**, 250401 (2016).

[8] S. Choi, J. Choi, R. Landig, G. Kucsko, H. Zhou, J. Isoya, F. Jelezko, S. Onoda, H. Sumiya, V. Khemani, *et al.*, Observation of discrete time-crystalline order in a disordered dipolar many-body system, *Nature* **543**, 221 (2017).

[9] J. Zhang, P. W. Hess, A. Kyprianidis, P. Becker, A. Lee, J. Smith, G. Pagano, I.-D. Potirniche, A. C. Potter, A. Vishwanath, *et al.*, Observation of a discrete time crystal, *Nature* **543**, 217 (2017).

[10] A. Kyprianidis, F. Machado, W. Morong, P. Becker, K. S. Collins, D. V. Else, L. Feng, P. W. Hess, C. Nayak, G. Pagano, *et al.*, Observation of a prethermal discrete time crystal, *Science* **372**, 1192 (2021).

[11] S. Pal, N. Nishad, T. Mahesh, and G. Sreejith, Temporal order in periodically driven spins in star-shaped clusters, *Physical review letters* **120**, 180602 (2018).

[12] J. Rovny, R. L. Blum, and S. E. Barrett, Observation of discrete-time-crystal signatures in an ordered dipolar many-body system, *Physical review letters* **120**, 180603 (2018).

[13] J. O’Sullivan, O. Lunt, C. W. Zollitsch, M. Thewalt, J. J. Morton, and A. Pal, Signatures of discrete time crystalline order in dissipative spin ensembles, *New Journal of Physics* **22**, 085001 (2020).

[14] J. Randall, C. Bradley, F. van der Gronden, A. Galicia, M. Abobeih, M. Markham, D. Twitchen, F. Machado, N. Yao, and T. Taminiau, Many-body-localized discrete time crystal with a programmable spin-based quantum simulator, *Science* **374**, 1474 (2021).

[15] H. Kefler, P. Kongkhambut, C. Georges, L. Mathey, J. G. Cosme, and A. Hemmerich, Observation of a dissipative time crystal, *Physical Review Letters* **127**, 043602 (2021).

[16] A. Greilich, N. E. Kopteva, V. L. Korenev, and M. Bayer, Exploring nonlinear dynamics in periodically driven time crystal: from synchronized to chaotic motion, *arXiv preprint arXiv:2406.06243* (2024).

[17] F. Iemini, A. Russomanno, J. Keeling, M. Schirò, M. Dalmonte, and R. Fazio, Boundary time crystals, *Physical review letters* **121**, 035301 (2018).

[18] C.-K. Chan, T. E. Lee, and S. Gopalakrishnan, Limit-cycle phase in driven-dissipative spin systems, *Physical Review A* **91**, 051601 (2015).

[19] H. Keßler, J. G. Cosme, M. Hemmerling, L. Mathey, and A. Hemmerich, Emergent limit cycles and time crystal dynamics in an atom-cavity system, *Physical Review A* **99**, 053605 (2019).

[20] B. Buča, J. Tindall, and D. Jaksch, Non-stationary coherent quantum many-body dynamics through dissipation, *Nature Communications* **10**, 1730 (2019).

[21] P. Kongkhambut, J. Skulte, L. Mathey, J. G. Cosme, A. Hemmerich, and H. Keßler, Observation of a continuous time crystal, *Science* **377**, 670 (2022).

[22] Y. Li, C. Wang, Y. Tang, and Y.-C. Liu, Time crystal in a single-mode nonlinear cavity, *Physical Review Letters* **132**, 183803 (2024).

[23] T. Liu, J.-Y. Ou, K. F. MacDonald, and N. I. Zheludev, Photonic metamaterial analogue of a continuous time crystal, *Nature Physics* **19**, 986 (2023).

[24] X. Wu, Z. Wang, F. Yang, R. Gao, C. Liang, M. K. Tey, X. Li, T. Pohl, and L. You, Dissipative time crystal in a strongly interacting rydberg gas, *Nature Physics* **20**, 1389 (2024).

[25] A. Greilich, N. E. Kopteva, A. N. Kamenskii, P. S. Sokolov, V. L. Korenev, and M. Bayer, Robust continuous time crystal in an electron–nuclear spin system, *Nature Physics* **20**, 631 (2024).

[26] B. Zhu, J. Marino, N. Y. Yao, M. D. Lukin, and E. A. Demler, Dicke time crystals in driven-dissipative quantum many-body systems, *New Journal of Physics* **21**, 073028 (2019).

[27] A. Pizzi, A. Nunnenkamp, and J. Knolle, Classical prethermal phases of matter, *Phys. Rev. Lett.* **127**, 140602 (2021).

[28] B. Ye, F. Machado, and N. Y. Yao, Floquet phases of matter via classical prethermalization, *Phys. Rev. Lett.* **127**, 140603 (2021).

[29] A. Pizzi, A. Nunnenkamp, and J. Knolle, Classical approaches to prethermal discrete time crystals in one, two, and three dimensions, *Phys. Rev. B* **104**, 094308 (2021).

[30] S. Dutta, S. Zhang, and M. Haque, Quantum origin of limit cycles, fixed points, and critical slowing down, *Phys. Rev. Lett.* **134**, 050407 (2025).

[31] E. T. Owen, J. Jin, D. Rossini, R. Fazio, and M. J. Hartmann, Quantum correlations and limit cycles in the driven-dissipative heisenberg lattice, *New Journal of Physics* **20**, 045004 (2018).

[32] M. Medenjak, B. Buča, and D. Jaksch, Isolated heisenberg magnet as a quantum time crystal, *Physical Review B* **102**, 041117 (2020).

[33] H. Labuhn, D. Barredo, S. Ravets, S. de Léséleuc, T. Macrì, T. Lahaye, and A. Browaeys, Tunable two-dimensional arrays of single rydberg atoms for realizing quantum ising models, *Nature* **534**, 667 (2016).

[34] H. Bernien, S. Schwartz, A. Keesling, H. Levine, A. Omran, H. Pichler, S. Choi, A. S. Zibrov, M. Endres, M. Greiner, *et al.*, Probing many-body dynamics on a 51-atom quantum simulator, *Nature* **551**, 579 (2017).

[35] P. Scholl, M. Schuler, H. J. Williams, A. A. Eberharter, D. Barredo, K.-N. Schymik, V. Lienhard, L.-P. Henry, T. C. Lang, T. Lahaye, A. M. Läuchli, and A. Browaeys, Quantum simulation of 2d antiferromagnets with hundreds of rydberg atoms, *Nature* **595**, 233 (2021).

[36] A. Browaeys and T. Lahaye, Many-body physics with individually controlled rydberg atoms, *Nature Physics* **16**, 132 (2020).

[37] A. M. Kaufman and K.-K. Ni, Quantum science with optical tweezer arrays of ultracold atoms and molecules, *Nature Physics* **17**, 1324 (2021).

[38] T. F. Gallagher, Rydberg atoms, in *Springer Handbook of Atomic, Molecular, and Optical Physics* (Springer, 1994) pp. 231–240.

[39] M. Saffman, T. G. Walker, and K. Mølmer, Quantum information with rydberg atoms, *Reviews of modern physics* **82**, 2313 (2010).

[40] S. Weber, C. Tresp, H. Menke, A. Urvoy, O. Firstenberg, H. P. Büchler, and S. Hofferberth, Calculation of rydberg interaction potentials, *Journal of Physics B: Atomic, Molecular and Optical Physics* **50**, 133001 (2017).

[41] M. Tanasittikosol, J. Pritchard, D. Maxwell, A. Gauget, K. Weatherill, R. Potvliege, and C. Adams, Microwave dressing of rydberg dark states, *Journal of Physics B: Atomic, Molecular and Optical Physics* **44**, 184020 (2011).

[42] S. Sevinçli and T. Pohl, Microwave control of rydberg atom interactions, *New Journal of Physics* **16**, 123036 (2014).

[43] D. Kurdak, P. R. Banner, Y. Li, S. R. Muleady, A. V. Gorshkov, S. Rolston, and J. Porto, Enhancement of rydberg blockade via microwave dressing, *arXiv preprint arXiv:2411.08236* (2024).

[44] R. Löw, H. Weimer, J. Nipper, J. B. Balewski, B. Butscher, H. P. Büchler, and T. Pfau, An experimental and theoretical guide to strongly interacting rydberg gases, *Journal of Physics B: Atomic, Molecular and Optical Physics* **45**, 113001 (2012).

[45] M. Morgado and S. Whitlock, Quantum simulation and computing with rydberg-interacting qubits, *AVS Quantum Science* **3** (2021).

[46] T. E. Lee, H. Häffner, and M. C. Cross, Antiferromagnetic phase transition in a nonequilibrium lattice of rydberg atoms, *Phys. Rev. A* **84**, 031402 (2011).

[47] M. Marcuzzi, E. Levi, S. Diehl, J. P. Garrahan, and I. Lesanovsky, Universal nonequilibrium properties of dissipative rydberg gases, *Phys. Rev. Lett.* **113**, 210401 (2014).

[48] F. Carollo and I. Lesanovsky, Exact solution of a boundary time-crystal phase transition: time-translation symmetry breaking and non-markovian dynamics of correlations, *Physical Review A* **105**, L040202 (2022).

[49] T. Nadolny, C. Bruder, and M. Brunelli, Nonreciprocal synchronization of active quantum spins, *Physical Review X* **15**, 011010 (2025).

[50] C. Carr, R. Ritter, C. Wade, C. S. Adams, and K. J. Weatherill, Nonequilibrium phase transition in a dilute rydberg ensemble, *Physical review letters* **111**, 113901 (2013).

[51] N. R. De Melo, C. G. Wade, N. Šibalić, J. M. Kondo, C. S. Adams, and K. J. Weatherill, Intrinsic optical bistability in a strongly driven rydberg ensemble, *Physical Review A* **93**, 063863 (2016).

[52] N. Šibalić, C. G. Wade, C. S. Adams, K. J. Weatherill, and T. Pohl, Driven-dissipative many-body systems with mixed power-law interactions: Bistabilities and temperature-driven nonequilibrium phase transitions, *Physical Review A* **94**, 011401 (2016).

[53] H. Weimer, Variational principle for steady states of dissipative quantum many-body systems, *Phys. Rev. Lett.* **114**, 040402 (2015).

[54] H. Weimer, A. Kshetrimayum, and R. Orús, Simulation methods for open quantum many-body systems, *Rev.*

Mod. Phys. **93**, 015008 (2021).

[55] R. Kubo, Generalized cumulant expansion method, Journal of the Physical Society of Japan **17**, 1100 (1962).

[56] F. Lackner, I. Březinová, T. Sato, K. L. Ishikawa, and J. Burgdörfer, High-harmonic spectra from time-dependent two-particle reduced-density-matrix theory, Physical Review A **95**, 033414 (2017).

[57] D. Plankensteiner, C. Hotter, and H. Ritsch, Quantum-Cumulants.jl: A Julia framework for generalized mean-field equations in open quantum systems, Quantum **6**, 617 (2022).

[58] S. Donsa, F. Lackner, J. Burgdörfer, M. Bonitz, B. Kloss, A. Rubio, and I. Březinová, Nonequilibrium correlation dynamics in the one-dimensional fermi-hubbard model: A testbed for the two-particle reduced density matrix theory, Physical Review Research **5**, 033022 (2023).

[59] W. Verstraelen, D. Huybrechts, T. Roscilde, and M. Wouters, Quantum and classical correlations in open quantum spin lattices via truncated-cumulant trajectories, PRX Quantum **4**, 030304 (2023).

[60] K. J. Kusmirek, S. Mahmoodian, M. Cordier, J. Hinney, A. Rauschenbeutel, M. Schemmer, P. Schneeweiss, J. Volz, and K. Hammerer, Higher-order mean-field theory of chiral waveguide QED, SciPost Phys. Core **6**, 041 (2023).

[61] See Supplemental Material for details on the cumulant expansion and the cluster mean-field simulations, a discussion of energies and fluctuations in the thermodynamic limit, and an analysis of atom heating due to spontaneous photon emission.

[62] J. Jin, A. Biella, O. Viyuela, L. Mazza, J. Keeling, R. Fazio, and D. Rossini, Cluster mean-field approach to the steady-state phase diagram of dissipative spin systems, Physical Review X **6**, 031011 (2016).

[63] F. Benatti, F. Carollo, R. Floreanini, and H. Narnhofer, Quantum spin chain dissipative mean-field dynamics, Journal of Physics A: Mathematical and Theoretical **51**, 325001 (2018).

[64] D. Goderis and P. Vets, Central limit theorem for mixing quantum systems and the ccr-algebra of fluctuations, Communications in Mathematical Physics **122**, 249 (1989).

[65] D. Goderis, A. Verbeure, and P. Vets, Non-commutative central limits, Probability Theory and Related Fields **82**, 527 (1989).

[66] D. Goderis, A. Verbeure, and P. Vets, Dynamics of fluctuations for quantum lattice systems, Communications in Mathematical Physics **128**, 533 (1990).

[67] A. F. Verbeure, *Many-body boson systems: half a century later* (Springer, 2010).

[68] F. Benatti, F. Carollo, R. Floreanini, and H. Narnhofer, Non-markovian mesoscopic dissipative dynamics of open quantum spin chains, Physics Letters A **380**, 381 (2016).

[69] F. Benatti, F. Carollo, R. Floreanini, and H. Narnhofer, Quantum fluctuations in mesoscopic systems, Journal of Physics A: Mathematical and Theoretical **50**, 423001 (2017).

[70] H. Levine, A. Keesling, A. Omran, H. Bernien, S. Schwartz, A. S. Zibrov, M. Endres, M. Greiner, V. Vuletić, and M. D. Lukin, High-fidelity control and entanglement of rydberg-atom qubits, Physical review letters **121**, 123603 (2018).

[71] Z. Wang, R. Gao, X. Wu, B. Buća, K. Mølmer, L. You, and F. Yang, Boundary time crystals stabilized by local dissipation and long-range interaction, to appear (2025).

Appendix A: Cumulant Expansion

We work in the Heisenberg picture, i.e., we perform the time evolution of the atomic operators consisting of $\sigma_{\alpha\beta}^{(i)}(t)$ and $\hat{n}_\alpha^{(i)}(t) = \sigma_{\alpha\alpha}^{(i)}(t)$, where $\sigma_{\alpha\beta}^{(i)}(0) = |\alpha\rangle_i\langle\beta|$ acts on the i th atom and $\alpha, \beta \in \{\downarrow, 0, \uparrow\}$. The master equation that governs the dynamics is

$$i\partial_t \hat{A} = [\hat{A}, \hat{H}] + i\mathcal{L}^*(\hat{A}), \quad (A1)$$

for an arbitrary operator \hat{A} , where

$$\mathcal{L}^*(\hat{A}) = \gamma \sum_i \left(\sigma_{0\downarrow}^{(i)} \hat{A} \sigma_{\downarrow 0}^{(i)} - \frac{1}{2} \{ \hat{n}_0^{(i)}, \hat{A} \} \right) \quad (A2)$$

is the dual of the Lindbladian from Eq.(2). Using a general notation, one can write the equation of motion for operator products as

$$\begin{aligned} & i\partial_t \left(\sigma_{\alpha_1\beta_1}^{(i_1)} \sigma_{\alpha_2\beta_2}^{(i_2)} \dots \sigma_{\alpha_N\beta_N}^{(i_N)} \right) \\ &= \left(\sigma_{\alpha_2\beta_2}^{(i_2)} \dots \sigma_{\alpha_N\beta_N}^{(i_N)} \left(\hat{K}_{\alpha_1+1\beta_1\alpha_1\alpha_1\beta_1\beta_1}^{(i_1)} - \hat{K}_{\alpha_1\beta_1-1\beta_1-1\alpha_1\beta_1\alpha_1}^{(i_1)} \right) \right. \\ & \quad \left. + \sum_{j \neq 1} (i_j, \alpha_j, \beta_j) \leftrightarrow (i_1, \alpha_1, \beta_1) \right) \\ & \quad - \text{h.c.}(\alpha_1 \leftrightarrow \beta_1, \alpha_2 \leftrightarrow \beta_2, \dots, \alpha_N \leftrightarrow \beta_N) \end{aligned} \quad (A3)$$

where

$$\begin{aligned} \hat{K}_{\alpha\beta\mu\nu\rho\tau}^{(i)} &\equiv \delta_{\beta\mu} \left(\Delta + i\delta_{\mu\downarrow} \frac{\gamma}{2} \right) \hat{\sigma}_{\alpha\mu+1}^{(i)} - \Omega_\mu \hat{\sigma}_{\alpha\beta}^{(i)} \\ &+ \frac{1}{2} \delta_{\tau\uparrow} \sum_{j \neq i} U_{ij} \hat{\sigma}_{\nu\rho}^{(i)} \hat{n}_\tau^{(j)}. \end{aligned} \quad (A4)$$

and we introduced addition of the spin indices $0 = \downarrow$, $+1 = \uparrow$, -1 . Operators containing indices outside of the ladder are defined to vanish, e.g., $\hat{\sigma}_{\alpha(\uparrow+1)}^{(i)} = \hat{0} \forall \alpha, i$. Moreover, we introduced the helper quantity

$$\Omega_\mu = \begin{cases} \Omega & \text{if } \mu = \downarrow \\ \omega & \text{if } \mu = 0 \\ 0 & \text{else.} \end{cases} \quad (A5)$$

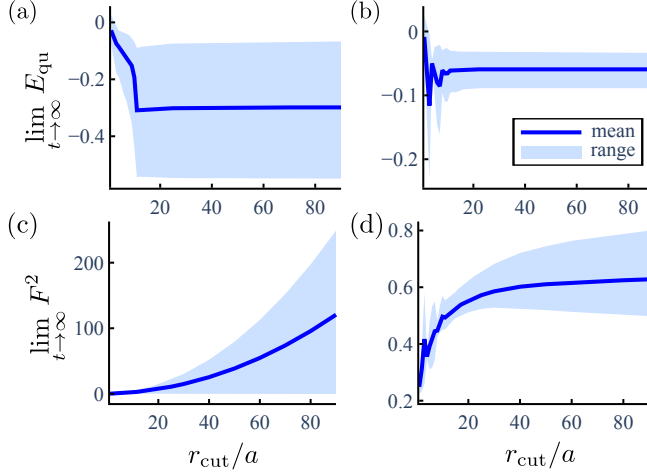


FIG. 5. (a), (b) Oscillation range of the (a)/(b) the correlation energy and (c)/(d) the normalized fluctuations in the long-time limit as a function of the cut-off radius in the thermodynamic limit. The panels on the left, i.e.,(a) and (c), show parameters within qCTC I while the panels on the right, i.e.,(b) and (d), show parameters within qCTC II. While the correlation energies remain finite, the fluctuations diverge. The kink in (a) comes from a more attractive periodic orbit that the observables start to follow.

From Eq.(A3), one can readily derive an equation of motion for the 2nd-order cumulants:

$$\begin{aligned} & i\partial_t \langle \hat{\sigma}_{\alpha\beta}^{(i)} \hat{\sigma}_{\alpha'\beta'}^{(i')} \rangle_c \\ &= \left(\langle \hat{\sigma}_{\alpha'\beta'}^{(i')} \hat{K}_{\alpha+1\beta\alpha\alpha\beta\beta}^{(i)} \rangle - \sigma_{\alpha'\beta'}^{(i')} \langle \hat{K}_{\alpha+1\beta\alpha\alpha\beta\beta}^{(i)} \rangle \right. \\ & \quad \left. - \left(\langle \hat{\sigma}_{\alpha'\beta'}^{(i')} \hat{K}_{\alpha\beta-1\beta-1\alpha\beta\alpha}^{(i)} \rangle - \sigma_{\alpha'\beta'}^{(i')} \langle \hat{K}_{\alpha\beta-1\beta-1\alpha\beta\alpha}^{(i)} \rangle \right) \right. \\ & \quad \left. + (\alpha \leftrightarrow \alpha', \beta \leftrightarrow \beta', i \leftrightarrow i') \right) \\ & \quad - c.c.(\alpha \leftrightarrow \beta, \alpha' \leftrightarrow \beta'). \end{aligned} \quad (A6)$$

Since \hat{K} contains 2nd-order terms, the 2nd-order cumulants depend on 3rd-order expectation values. To obtain a closed set of equations, we approximate the latter by two-body terms, neglecting the third-order cumulant:

$$\begin{aligned} & \langle \hat{\sigma}^{(n_1)} \hat{\sigma}^{(n_2)} \hat{\sigma}^{(n_3)} \rangle \\ & \approx \langle \hat{\sigma}^{(n_1)} \hat{\sigma}^{(n_2)} \rangle \langle \hat{\sigma}^{(n_3)} \rangle + \langle \hat{\sigma}^{(n_1)} \hat{\sigma}^{(n_3)} \rangle \langle \hat{\sigma}^{(n_2)} \rangle \\ & \quad + \langle \hat{\sigma}^{(n_1)} \rangle \langle \hat{\sigma}^{(n_2)} \hat{\sigma}^{(n_3)} \rangle - 2 \langle \hat{\sigma}^{(n_1)} \rangle \langle \hat{\sigma}^{(n_2)} \rangle \langle \hat{\sigma}^{(n_3)} \rangle, \end{aligned} \quad (A7)$$

where we omitted the spin indices.

1. Thermodynamic Limit

In the thermodynamic limit, we can make use of the homogeneity of the system to only simulate one set of

single-site equations corresponding to an arbitrary atom, which we label with the index 0 in the following. However, the single-site operators are coupled to infinitely many two-site operators, see Eq.(A4) for example. Performing a cumulant expansion (cf. Eq.(5)), the interaction term of the single-site operators can be rewritten

$$\sum_{j \neq 0} U_{0j} \langle \hat{\sigma}_{\alpha\beta}^{(0)} \hat{n}_{\uparrow}^{(j)} \rangle = \chi \sigma_{\alpha\beta} n_{\uparrow} + \sum_{j \neq 0} U_{0j} \langle \hat{\sigma}_{\alpha\beta}^{(0)} \hat{n}_{\uparrow}^{(j)} \rangle_c, \quad (A8)$$

where we used the translational symmetry in the thermodynamic limit and introduced $\sigma_{\alpha\beta} \equiv \sigma_{\alpha\beta}^{(0)}$. From Eq.(A8), one sees immediately that the mean-field equations are nonlinear and agnostic to the microscopic details of the potential (they only depend on the effective nonlinearity χ).

To simulate the dynamics in the thermodynamic limit despite the infinite number of 2nd-order correlations appearing in Eq.(A8), we use that the Rydberg potential decays as a function of the distance between sites, allowing us to cut off the sum appearing in the second term. In Figure 5(a) and (b), we show the oscillation ranges of the correlation energy (i.e., the second term in Eq.(A8) for $\alpha = \beta = \uparrow$, see Eq.(10)) in the limit of long simulation times as a function of where we choose the cutoff. For both time-crystalline phases, we find that (1) the correlation energy oscillates between finite values and (2) the sum has converged when cutting it off after $r_{\text{cut}} = 40a$, where a is the lattice constant.

As discussed in the main text, the normalized fluctuations

$$F^2 = n_{\uparrow} - n_{\uparrow}^2 + \sum_{j \neq 0} \langle \hat{n}_{\uparrow}^{(0)} \hat{n}_{\uparrow}^{(j)} \rangle_c, \quad (A9)$$

diverge as a function of N for finite systems and, therefore, also do not converge as function of r_{cut} , as seen in Figure 5(c) and (d).

Appendix B: Cluster Mean-Field Approach

Another approach to include short-range correlations is the cluster mean-field approach. Hereby, the lattice is grouped into small connected clusters \mathcal{C}_i that are assumed to factorize, i.e.,

$$\hat{\rho} = \otimes_i \hat{\rho}_{\mathcal{C}_i}. \quad (B1)$$

Substituting this relation into the master equation and tracing over all clusters except one (denoted by \mathcal{C}), we obtain

$$\begin{aligned} i\partial_t \hat{\rho}_{\mathcal{C}} &= \sum_{j \in \mathcal{C}} \left([\hat{h}_j, \hat{\rho}_{\mathcal{C}}] + i\hat{\mathcal{L}}_j(\hat{\rho}_{\mathcal{C}}) \right) \\ & \quad + \frac{1}{2} \sum_{j, k \in \mathcal{C}} U_{jk} [\hat{n}_{\uparrow}^{(j)} \hat{n}_{\uparrow}^{(k)}, \hat{\rho}_{\mathcal{C}}] \\ & \quad + \sum_{j \in \mathcal{C}, k \notin \mathcal{C}} U_{jk} [\hat{n}_{\uparrow}^{(j)} \hat{n}_{\uparrow}^{(k)}, \hat{\rho}_{\mathcal{C}}] \end{aligned} \quad (B2)$$

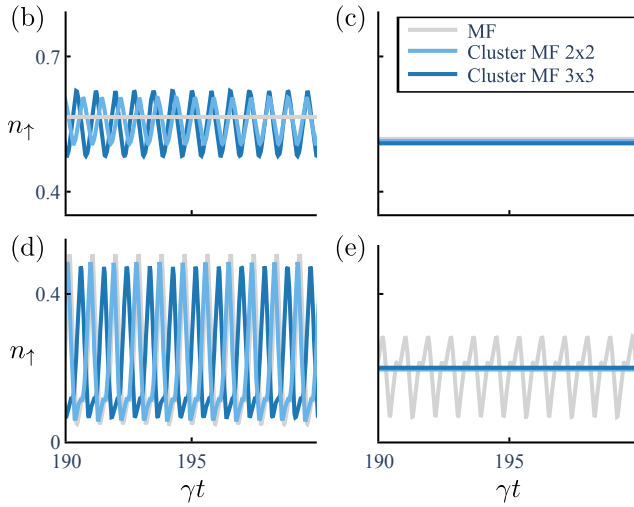


FIG. 6. Dynamics of the spin-up population at large simulation times for different cluster sizes. The parameters in (b)-(d) correspond to the four points labeled with these letters in the phase diagram in Figure 2a. The cluster mean-field simulations are in qualitative agreement, deviating from the simple mean-field prediction.

where we used the cyclic property of the trace and introduced the single-particle Hamiltonian

$$\hat{h}_i = -\Delta \left(\hat{n}_0^{(i)} + \hat{n}_\uparrow^{(i)} \right) + \left(\Omega \hat{\sigma}_{\downarrow 0}^{(i)} + \omega \hat{\sigma}_{0\uparrow}^{(i)} + \text{h.c.} \right) \quad (\text{B3})$$

as well as the single-particle Lindbladian

$$\hat{\mathcal{L}}_{(i)}(\hat{A}) = \gamma \left(\hat{\sigma}_{\downarrow 0}^{(i)} \hat{A} \hat{\sigma}_{0\downarrow}^{(i)} - \frac{1}{2} \{ \hat{n}_0^{(i)}, \hat{A} \} \right). \quad (\text{B4})$$

While the first two lines in Eq.(B2) give the exact solution for the cluster \mathcal{C} , the term in the last line accounts for the mean-field interaction with the atoms in the remaining clusters. Practically, this means that we simulate the exact dynamics of the cluster including a self-consistent detuning

$$\tilde{\Delta}_j = \sum_{k \notin \mathcal{C}} U_{jk} n_\uparrow^{(k)}, \quad (\text{B5})$$

where $j \in \mathcal{C}$. It is intuitively clear that we approach the exact solution as the cluster size grows. Due to the three-level structure of our particles, we are limited to clusters of size 2×2 and 3×3 . However, the dynamics corresponding to the two cluster sizes are in qualitative agreement, see Figure 6

Appendix C: Trap Heating by Spontaneous Decay

One of the main sources of loss in a tweezer experiment comes from heating due to decays of the intermediate state. A measure for the amount of dissipation is the

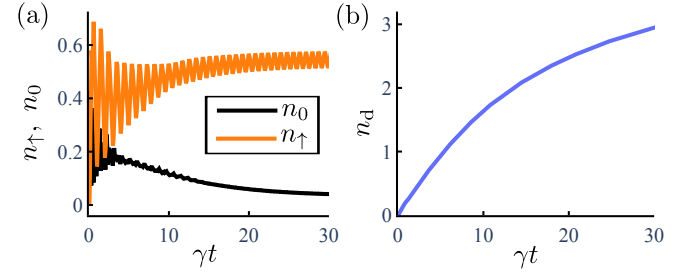


FIG. 7. (a) Dynamics of the Rydberg and the intermediate-state population at large simulation times as predicted by a cumulant expansion. The intermediate-state population oscillates with an amplitude that is not resolved in this plot. (b) Number of decays per atom as a function of time. Parameters are taken from the qCTC II phase.

number of decays per atom, i.e., in the thermodynamic limit,

$$n_d(t) = \gamma \int_0^t n_0(\tau) d\tau. \quad (\text{C1})$$

As shown in Figure 7(a), the population of the intermediate state is quite low in the qCTC II phase. Consequently, few decays happen and one should be able to observe multiple oscillations of the Rydberg population before the losses due to heating lead to a deterioration of the experimental data, see Figure 7(b). Note that the population of the intermediate state also oscillates in Figure 7(a) but with a smaller amplitude.